A rapid method for analyzing the chemical bond from energy densities calculations at the bond critical point

Hailong Yang, P. Boulet, Marie-Christine Record

A rapid method for analyzing the chemical bond from energy densities calculations at the bond critical point

Hailong Yang [1,2], Pascal Boulet[1], Marie-Christine Record[2]

[1] MADIREL, Aix-Marseille Université, CNRS, Marseille 13013, France

[2]IM2NP, Aix-Marseille Université, CNRS, Marseille 13013, France

ABSTRACT

The quantum theory atoms in molecules (QTAIM) method has been used in this paper to characterize various bonding interactions in molecules and solid compounds. By using DFT-PAW calculations, complete electron density Laplacian distributions have been obtained and related to energies densities calculated at the bond critical points. From the analysis of these results a simple and rapid method, based solely on local energies densities calculations, is proposed to diagnose the bonding state, the polarizability and the deformation of the charge distribution.

KEYWORDS

Chemical bond, electron density topological properties, DFT, QTAIM

I. Introduction

X-ray diffraction, as a unique tool for obtaining the experimental charge density in crystals, can be helpful in the study of chemical bonding in solids [1]. By analyzing the X-ray determined charge densities with the quantum theory of atoms in molecules (QTAIM), the interactions or bonding between atoms can be quantitatively interpreted in the real space [1-2]. The information obtained by combining theory and experiment allows for a better description of the atomic interactions, making the parallel analysis of theoretical and experimental charge density to become common [1,3-13], especially as the QTAIM theory is rather independent from the basis set and the level of the quantum theoretical method used [14-16].

The topological definition of a bonded interaction is based on the existence of a bond path (BP), the charge density being a maximum along the BP with respect to any neighboring line. BP is known as the atomic interaction line in the topological analysis of the electron density ρ(r) distribution. It is associated with all kinds of interactions, going from weak ones, such as intermolecular [7,17], Van der Waals [18], secondary ones between ions [19,20], nonbonding [21,22], and hydrogen bonds [23,24], to strong interactions, namely metal-metal [10,25-27], ionic [27-30], and covalent bonds [6,27-32], and also other kinds of uncommon bonding, for instance charge-shift bonding [28-29,33]. For intermolecular interactions, the

Laplacian of the electron density $\nabla^2\rho(r)$ allows one to define Lewis acid and base sites [17] and reveal directional 'key-lock' interactions corresponding to molecular recognition [7], which contributes to construct layered structures [34]. The investigation of the energy densities at the bond critical point (BCP) and of $\rho(r)$ and $\nabla^2\rho(r)$ for solids and noble gas, offers recognition of van der Waals interactions as the result of a weak accumulation of electron density between the nuclei, leading to small binding energy [18,30]. The ionic secondary interactions (e.g. alike ions in halides), caused by a large cation/anion size ratio and small unit cell, correspond, according to the analysis of existing BCPs, to energetically stabilized nonbonding repulsive interactions [19-22] and have properties at the BCP similar to that of closed-shell interaction of hydrogen bonds [23,24]. The metal-metal bonds in bulk metals have flat $\rho(r)$ in the valence region and own a partial covalence degree [10,25-27]. The bond metallicity can be evaluated with the ratio $\xi_b=\rho_b/\nabla^2\rho_b$, b standing for the BCP [35,36]. The typical ionic bonds and covalent bonds are pure closed-shell interactions and shared-shell interactions, respectively. The polarization of bonds can be described by the deviation of the BCP from the midpoint [29] and the deviation of ρ_b from cylindrical symmetry, the latter deviation being defined by the bond ellipticity value $(\varepsilon=\lambda_1/\lambda_2)-1$, with λ_1 and λ_2 the principal curvatures of ρ_b [6,32]. The Laplacian distribution can state that ionic binding and covalent one are generated by the charge localized on one of the nuclei and an increased density equally shared between the nuclei, respectively [37]. The charge-shift bonding has a large ρ_b and a large positive $\nabla^2\rho_b$, which makes this interaction unclassifiable by the standard criteria [28,29,33].

However, the chemical bonding analysis by the QTAIM tool is limited by two problems. One is the Laplacian distribution of heavy elements and transition metals missing the complete shell structure of isolated atom, either because the last atomic shell is not resolved or $\nabla^2\rho(r)$ lacks charge concentration region as it is always positive there. The other is the sign of $\nabla^2\rho(r)$ belonging to the intermediate region between regions of pure closed-shell interactions and shared-shell interactions, which is quite indeterminate due to diffuse atomic valence density, causing low $\rho(r)$ and $\nabla^2\rho(r)$ magnitudes in the bonding regions [38,39]. Therefore, using the simple criterion of $\nabla^2\rho(r)$ at one point to characterize or classify the bonding in these two cases becomes particularly deceiving for intermediate region.

In this paper, we investigate the relations between the integral distribution of atomic interactions (Valence Shell Charge Concentrations) combined with the local virial theorem and the energy densities (local properties) at the bond critical point in order to propose a method to directly characterize the bonding interactions from the local properties. The density functional theory (DFT) has been used to calculate the Laplacian of the electron density for the outermost valence region of heavy atoms. And, in order to characterize and classify a large panel of bonds, the analysis of chemical bonding by the QTAIM tool has been carried out on various chemical systems going from molecules to ternary solid compounds.

II. Computational Methods

Density functional theory (DFT) calculations were performed using the QUANTUM ESPRESSO (QE) simulation package [40,41]. The electronic exchange-correlation energy was treated by the generalized gradient approximation (GGA) using the Perdew-Burke-Ernzerhof (PBE) functionals [42] and the interaction between ions and core electrons was described by the projector augmented wave (PAW) method [43]. The scalar relativistic corrections have been accounted for in the PAW pseudopotentials as most of the relativistic effects on the electron density topology can be recovered at this level of theory [44]. The electron density for all the systems of interest was calculated with a kinetic energy cutoff for wavefunctions of 48 Ry and the Monkhorst-Pack procedure was used to generate k-points for the Brillouin-zone sampling. For the molecular system H_2O_2, calculations were also performed with the ORCA program (version 4.2.1) [45,46] at the Hartree-Fock level with both the STO-3G and Def2-TZVPPD atomic basis sets [47-50], and at the B3LYP, PBE and the reference CCSD(T) levels with the Def2-TZVPPD ones.
The electron density was subsequently analyzed with the program Critic2 [51] that implements Bader's Quantum Theory of Atoms in Molecules (QTAIM). In this work, the model used in Critic2 for the kinetic energy density G(r) calculation is based on the Thomas-Fermi equation with the semi-classical gradient correction proposed by Kirzhnits [52,53]. On this basis, Abramov [54] proposed a simple approximate expression for directly relating G(r) to ρ(r):

$$G(r) = \frac{3}{10}(3\pi^2)^{\frac{2}{3}}\rho(r)^{\frac{5}{3}} + \frac{1}{72}\frac{[\nabla\rho(r)]^2}{\rho(r)} + \frac{1}{6}\nabla^2\rho(r) \qquad (1)$$

In spite of a weak accuracy for typical shared interactions of eq.(1), this equation gives a relatively accurate description in the medium-range distance (≈ 1-4 a.u., from BCP to nucleus) of G(r). It was found that the G(r) values from eq.(1) are nearly quantitative for closed-shell interactions [24,55]. However the accuracy of eq.(1) can become weak for typical shared interactions [38], as will be confirmed hereafter in the case of H_2O_2. The local virial theorem [2] describes the effects of chemical bonding by local energy densities through $\nabla^2\rho(r)$:

$$\frac{1}{4}\nabla^2\rho(r) = 2G(r) + V(r) \qquad (2)$$

$$G(r) + V(r) = H(r) \qquad (3)$$

where G, V and H are the kinetic, potential and total energy densities, respectively. Accordingly, the analysis of $\nabla^2\rho(r)$ gives evidence of charge concentration ($\nabla^2\rho(r)<0$) or depletion ($\nabla^2\rho(r)>0$) in the bonding region without resorting to a reference density. The charge depletion can also lead to a local charge accumulation when $|V(r)|/G(r)>1$, which gives rise to a relatively stable bonding dominated by the

potential energy. The V(r) virial field dominated by the potential energy density in a system is the virial of the Ehrenfest force exerted on the electron density. Combining the virial theorem of energy with force, H(r)<0 and H(r)>0 indicate stable bonding and pure closed-shell interaction, respectively [30,38,56]. Thus, the properties of H(r) or H(r)/ρ(r) can provide a good compensation for the weakness of the Laplacian distribution for a specific interaction.

On the basis of the properties of Laplacian distribution and total energy density, the local properties at the BCP can be used to analyze a series of interactions in solids or crystals between pure closed-shell interactions and shared-shell interactions. According to eq.(3),

$$\frac{H_b}{\rho_b} = \frac{G_b}{\rho_b}\left(1 - \frac{|V_b|}{G_b}\right) \qquad (4)$$

when $\nabla\rho$ vanishes at BCP, G_b, V_b and H_b are only related to ρ_b and $\nabla^2\rho_b$ from eq.(1) and eq.(2). Eq.(4) displays the variation of H(r)/ρ(r) along with $|V_b|/G_b$: the former indicator, the bond degree first introduced by Espinosa [57], stands for the total energy per electron related to the total electronic pressure, the latter one exhibits the competition between potential energy and kinetic energy for bonding formation. These two indicators corresponding to specific characteristics of bonding can be used for the bonding classification. At the same time, the kinetic energy per electron G_b/ρ_b is related to the variation tendency of H_b/ρ_b vs $|V_b|/G_b$, which is also an important parameter for classification of bonding [27,38,57]. We shall mention that, eq.(4) is valid only if the Kirzhnits approximation holds.

For the $CuSbSe_2$ compound, in the calculation of the energies densities, we have used both the optimized electron density and the promolecular one, which consists in the sum of atomic densities (IAM - independent atom model).

III. Results and Discussion

III.1. Electron density and its Laplacian distribution in chemical bondings

According to radial density function calculations, in the periodic table from Sc to Ge, the Laplacian distribution of the N shells becomes indistinguishable from that of the M ones [58], and the outermost atomic shell charge concentration of transition metals are missing. Many methods have been considered to explore this problem and without exception they all have encountered the same situation, e.g. in Co [4,59], Fe [10,59], Cr and Cd [10], Cu [25,60], W [60], Ti, Mn, Ni and Mo [59].

Fig.1 depicts the Laplacian distribution of bulk Cu [61] calculated from DFT-PAW based method that shows a four shells structure corresponding to charge concentration and depletion, with the spherical outermost valence shell regions of neighbouring atoms intersecting with each other and giving rise to an

interconnected valence shell charge concentration (VSCC) along the BP confined in a volume with a convex lens shape. This highly delocalized network of valence regions is responsible for the binding in the metallic system and for its conductive properties. The characteristics of metal-metal bond are then fully displayed by the Laplacian distribution map.

Although from As to Kr the M and N shells are separated, the sign of the Laplacian indicates that the outermost shell is charge depleted [4,58]. Similar trends of lacking the outermost charge concentration region were observed for the subsequent rows [62]. Further investigations with the DFT-PAW method show that the Laplacian distribution of both the nearest Se neighbours and second-nearest Se ones in metalloid bulk Se [63] exhibits a separation of the outer valence regions into two shells (Fig.2). The charge mostly corresponds to a localized accumulation slightly towards the inner shell, leading to inconspicuous charge concentration in the outermost spherical shell and quite indeterminate sign of the Laplacian there. Interestingly, the VSCC of nearest Se neighbours present a butterfly-type pattern around the BCP with a continuous charge concentration at the BCP induced by nearby parts of two spherical valence regions, reflecting a covalent character, and wings constituted of two localized valence regions. This bonding exemplifies the fulfilment of the virial equilibrium ($|V_b|/G_b \approx 2$, Tab.1) for a covalent bond dominated by the potential energy in the whole interatomic region (Fig.2(a)). In the interaction between second-nearest Se neighbours, the local charge accumulates along the BP though away from the BCP (Fig.2(b)), resulting in extremely weakly negative H_b and $|V_b|/G_b$ close to 1 (Tab.1). Combined with the dispersive H(r) distribution, it can be figured out to be a closed-shell interaction without charge transfer, and relatively stable as dominated by the potential energy (Fig.2(b)). This interaction could be related to a key-lock arrangement of the Se lone-pairs, similar to that reported in GeSe by Sist et al. [64].

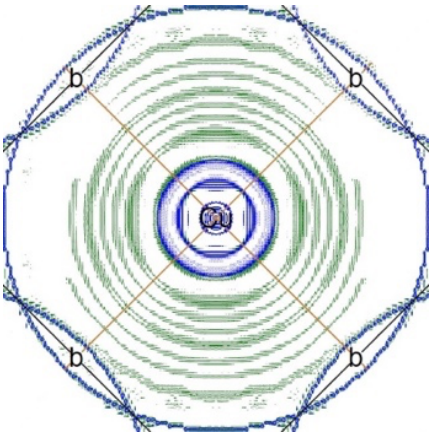

Figure 1. Laplacian distribution of Cu-Cu metal bonding in bulk Cu. Green and blue contour curves stand for positive and negative values, respectively. ‘b’ corresponds to the bond critical point.

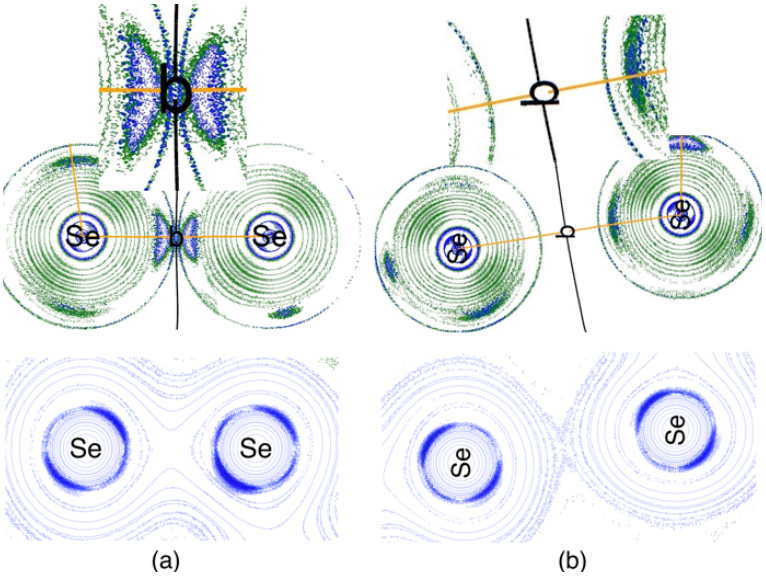

Figure 2. Distributions of $\nabla^2\rho(r)$ (top) and H(r) (bottom) of Se-Se bonding in bulk Se: (a) nearest neighbours; (b) second-nearest neighbours. Colour code: see Figure 1.

The distributions of $\nabla^2\rho(r)$ and H(r) have also been calculated for heavier elements of the fifth row by DFT-PAW method. The outermost spherical valence regions are displayed for bulk metalloid Sb [65] in Fig.3. The Laplacian distribution of nearest Sb neighbours shows some charge accumulation between adjacent valence regions around the BCP (Fig.3(a)), while the positive values of $\nabla^2\rho_b$ and $|V_b|/G_b<2$ (see Tab.1) are arguments against the classification of this bonding in the shared-shell interaction type. This statement is confirmed from Fig.3(a), which allows us to suggest that the charge accumulation around the BCP for the nearest Sb-Sb bonding does not originate from a real, shared charge density but from the diffusion of very close outermost shell charge concentrations. Regarding the second-nearest Sb neighbours (Fig.3(b)), in spite of a wide H(r) distribution between the atoms, the VSCCs are away from the interatomic surface. This behavior is similar to that described above for Se: the charge density depletion could be due to a key-lock arrangement of the lone-pairs. Moreover, the second-nearest Se-Se bonding indicates a more contracted charge accumulation towards the BP than the second-nearest Sb-Sb bonding despite the fact that both have very close values of ρ_b (Tab.1).

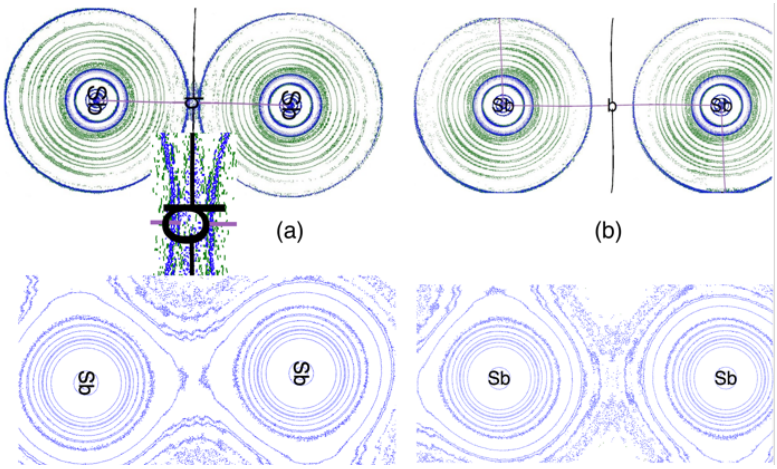

Figure 3. Distributions of $\nabla^2\rho(r)$ (top) and H(r) (bottom) of Sb-Sb bonding in bulk Sb: (a) nearest neighbours; (b) second-nearest neighbours.

The peculiar charge-shift bonding of O-O in H_2O_2 molecule [66] is dramatically exhibited in Fig.4. This bonding has the following remarkable characteristics: i) the whole VSCC is interrupted around BCP; ii) the inner charge shifts towards outer shell charge concentration. These characteristics are well in agreement with both the Pauli repulsion weakening the covalency of the bond and a large pressure exerted on the electron density (large H_b/ρ_b, Tab.1), leading to a decrease of the kinetic energy without significantly affecting the potential energy ($|V_b|/G_b$ slightly less than 2, line 6 of Tab.1). In addition both the $\nabla^2\rho(r)$ and H(r) distributions display localized electrons and/or non-bonded atoms bearing lone pairs (Fig.4) [67-69].

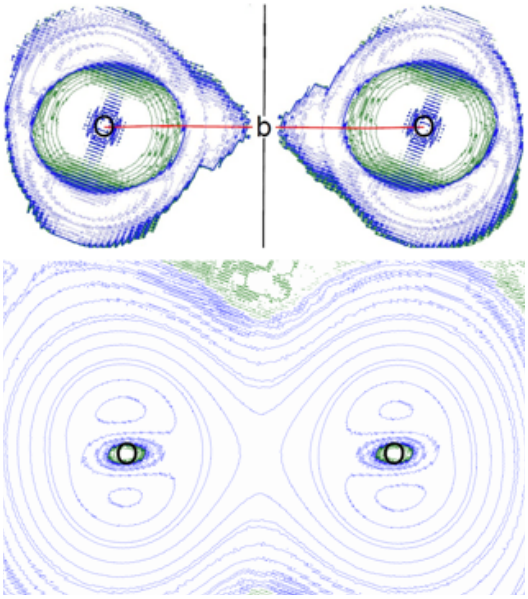

Figure 4. Distributions of $\nabla^2\rho(r)$ (top) and H(r) (bottom) of O-O bonding in H_2O_2 molecule.

All the above calculations have been performed using plane waves and the energy densities using the Kirzhnits approximation. However, as shown in Ref [38], this approximation is weakly accurate for shared interactions for *in vacuo* systems, the deviation reaching up to 300% in some cases. Therefore, in order to validate our results, we have performed additional calculations for H_2O_2 using localized molecular orbital approach, which allows us to obtain nearly true energy densities. The results are given in Table 1. The Laplacian value obtained with the state-of-the-art reference CCSD(T) method amounts to 0.017856 e.Å^{-5} whereas that of B3LYP is intermediate between the latter and that obtained with PBE. This shows that, the exact exchange interaction is an important ingredient to obtain accurate electron density curvatures. The Hartree-Fock level yields a negative Laplacian value at the BCP (O-O^b and O-O^c in Table 1), which is obviously wrong and caused by the lack of electronic correlation. Compared to B3LYP (O-O^d), PBE (O-O^e) and CCSD(T) (O-O^f) energy densities, those obtained with the Kirzhnits approximation (O-O^a) are about 100% off. However, the signs of the values given by this approximation agree with those of the reference values, therefore qualitative interpretations of VSCC can be conducted with this approximation.

Due to the absence of shared interaction in the inorganic solids investigated hereafter, the energy densities have been calculated in the realm of the Kirzhnits approximation.

Table 1. Energy density parameters at BCPs

Interaction	ρ_b	$\nabla^2\rho_b$	G_b	V_b	H_b	H_b/ρ_b	G_b/ρ_b	$\lvert V_b\rvert/ G_b$	Distance
Cu-Cu	0.040387	0.044567	0.019501	-0.029949	-0.010448	-0.258697	0.482853	1.535767	2.552
Se-Se[1]	0.089750	-0.045870	0.051443	-0.103206	-0.051764	-0.576758	0.573181	2.006220	2.420
Se-Se[2]	0.020081	0.040622	0.011030	-0.011904	-0.000874	-0.043524	0.549275	1.079238	3.235
Sb-Sb[1]	0.049389	0.005384	0.019986	-0.038627	-0.018640	-0.377412	0.404665	1.932703	2.945
Sb-Sb[2]	0.020743	0.008917	0.005982	-0.009736	-0.003753	-0.180929	0.288386	1.627549	3.444
O-O^a	0.270780	0.146054	0.349791	-0.663068	-0.313278	-1.156860	1.291696	1.895614	1.465
O-O^b	0.328205	-0.302567	0.227321	-0.530284	-0.302963	-0.923091	0.692619	2.332754	1.396
O-O^c	0.344644	-0.330036	0.226887	-0.536284	-0.309396	-0.897727	0.658323	2.363657	1.386
O-O^d	0.278853	0.066722	0.194687	-0.372694	-0.178006	-0.638352	0.698170	1.914321	1.449
O-O^e	0.267436	0.127763	0.191311	-0.350682	-0.159371	-0.595920	0.715353	1.833043	1.464
O-O^f	0.270155	0.017856	0.183455	-0.362446	-0.178991	-0.662548	0.679072	1.975667	1.460

[1] nearest neighbors. [2] second-nearest neighbors.

G_b, V_b and H_b are determined from the following methods: [a] Kirzhnits approximation. [b] HF/STO-3G. [c] HF/Def2-TZVPPD. [d] B3LYP/Def2-TZVPPD. [e] PBE/Def2-TZVPPD. [f] CCSD(T)/Def2-TZVPPD. The units are: electrons/bohr^3 for ρ_b, electrons/bohr^5 for $\nabla^2\rho_b$, Hartree/bohr^3 for V_b, G_b and H_b and Å for distances.

III.2. Analysis of chemical bondings using energy densities at the bond critical point

The energy density parameters H_b/ρ_b, $|V_b|/G_b$, G_b/ρ_b at bond critical points are referred in this work as local properties. These parameters are linked together by eq.(4), which can be regarded, when G_b/ρ_b is constant, as an affine equation $y=a_0+a_1.x$, with $y= H_b/\rho_b$ and $x=|V_b|/G_b$. Then the corresponding straight line passes through the point (1, 0) and its slope satisfies the relation $|a_1|=a_0= G_b/\rho_b$. Some examples for bonds in molecules and complexes are given in Fig.5(a). As can be seen, the H-F bonds, both for isolated molecule and in complexes, and Li-C bonds in methyllithium polymers obey this affine relation. Since the number of electrons in bonding molecular orbital linearly decreases when the interatomic distance increases (see Fig.5(b)), at least around the bond equilibrium state, the slope $|a_1|$ of these lines is related to the evolution of the charge density, which corresponds to a deformation of the electronic shells. The delineation of the electronic shell results from an accommodation between potential and kinetic energies that can be regarded as a pressure exerted on an electron by the other electrons or by an electron on the other ones, respectively. Therefore the slope $|a_1|$ reflects resistance to deformation of the electronic shells (reciprocal of polarizability) under pressure and can be considered as the rigidity of the interaction between atoms. This statement agrees with the larger G_b/ρ_b ratio reported in literature for pure closed-shell interaction [30, 38, 39, 57, 70]. Hence for a specific interaction that bears a specific polarization, the linear characteristic of H_b/ρ_b vs $|V_b|/G_b$ reflects a linear evolution between deformation of charge distribution and interatomic distance, the G_b/ρ_b ratio being related to the polarization of the interaction. Larger G_b/ρ_b ratio ($|a_1|$) corresponds to greater charge separation and as a consequence to lower polarizability.

In general, the bonding environment is more complex in solids or crystals due to their complex structures, not only related to bond lengths but also to other factors, such as coordination.

(a)

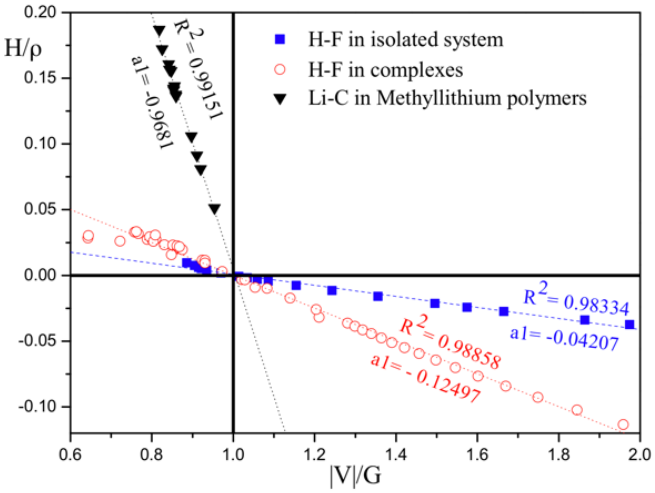

(b)

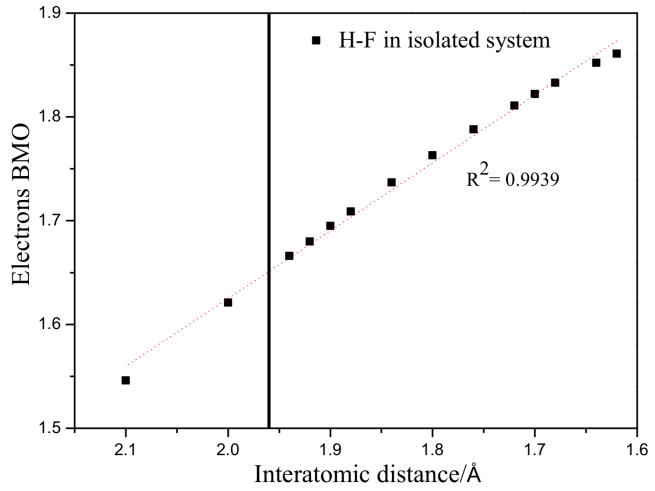

Figure 5. (a) H_b/ρ_b vs $|Vb|/G_b$ for H-F and Li-C bonding; (b) number of electrons in bonding molecular orbital (BMO) vs d(H···F). R^2 and a_1 are the regression coefficient and the slope of the fitted line, respectively. The numerical data are from literature Ref. 57 and Ref. 59.

As can be seen in Fig. 6, the evolution of H_b/ρ_b versus $|V_b|/G_b$ at the BCPs of As-O interactions in As_2O_3, AsO_2 and As_2O_5 is obviously deviating from the linearity. However, if one restricts to the closed-shell interactions ($H_b>0$) of As-O, the H_b/ρ_b values are almost aligned. As mentioned above, in case of different interactions (existing here in different compounds), the linearity is observed when the polarization of the charge distribution is similar. This agrees with the fact that these interactions all correspond to interlayer As-O ones which contribute to the formation of layered structures, with large interatomic distance (>2.9 Å) and high directivity which can be related to their low rigidity (low $|a_1|$).

As for the intralayer As-O interactions, since they belong to three different kinds of polyhedrons, namely $[AsO_3]$ pyramid, $[AsO_6]$ octahedron and $[AsO_4]$ tetrahedron, they can be divided into three groups (see Fig.6). These three groups have very different bonding characteristics including bond length, bond angle

and coordination. Generally, the bond length increases from tetrahedron to pyramid then to octahedron, this observation being in agreement with the corresponding increase of H_b/ρ_b (Fig.6). The observed dispersion of the values at the BCPs for a same polyhedron is caused by the occurrence of different bond lengths, which results from different polarizations of the charge distribution. Reversibly, since the shortest two As-O bonds in the octahedron of As_2O_5 have a G_b/ρ_b value close to that of As-O bonds in pyramids (Fig.6) these bonds should have similar rigidity. In an energy domain fulfilling a linear evolution between deformation of charge distribution and interatomic distance, similar G_b/ρ_b for two different interactions involving the same atoms should reflect similar polarization and as a consequence similar bonding environment.

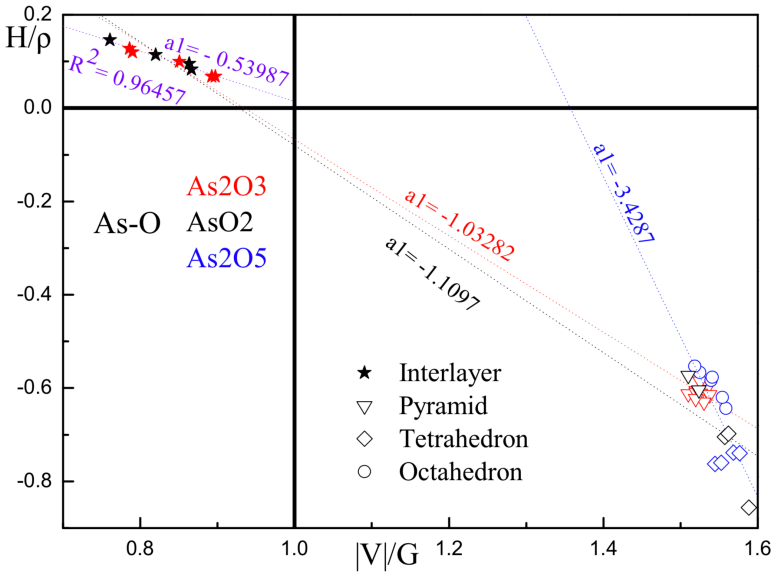

Figure 6. H_b/ρ_b vs $|V_b|/G_b$ for As-O bonding. The numerical data are from literature Ref. 18.

Ternary compounds bear even more complex interatomic interactions. We have investigated intermediate compounds of the Cu-Sb-Se system, namely the well established $CuSbSe_2$ (space group Pnma, number 62) [71], Cu_3SbSe_3 (space group Pnma, number 62) [72], Cu_3SbSe_4 (space group I-42m, number 121) [73] ones and the predicted Cu_4SbSe_5 (space group I-4, number 82), and $Cu_{12}Sb_4Se_{13}$ (space group $P2_1$, number 4) ones [74], hereafter named Se2, Se3, Se4, Se5 and Se13, respectively. The Sb-Se interactions characteristics, H_b/ρ_b vs $|V_b|/G_b$, are plotted in Fig.7(a). It can be seen that they are linearly dependent and the corresponding straight line passes through the point (1, 0). This result implies that the Sb-Se interactions in Cu-Sb-Se ternary system have similar bonding environment almost determined by interatomic distances, being consistent with the linear relationship between interatomic distances and the distances of BCPs to the point (1, 0) (Fig.7(b)), despite the existence of both [$SbSe_3$] pyramid and [$SbSe_4$] tetrahedron. The maximal deviation from this line occurs for Se2 at point 3, which corresponds to a longer Sb-Se bond

(3.165 Å) in the [$SbSe_3$] pyramidal unit. Moreover, one can see from the distribution of $\nabla^2\rho(r)$ and H(r) (Fig.8) that if charge transfer occurs at point 4, this feature hardly happens at point 3.

A comparison between interactions at point 1 and 2 (Fig.9), both dominated by the kinetic energy in the bonding region (Fig.7 (a)), shows a more pronounced closed-shell character at point 1, being farther away from the point (1, 0). Indeed the algebraic distance from BCP to the point (1, 0) in the map relating H_b/ρ_b to $|V_b|/G_b$ corresponds to the degree of closed-shell interaction for the negative values and to the charge sharing magnitude for the positive ones. In order to check that eq.(4) allows for detecting similar bonding environments instead of depending only on the interatomic distance, we have also calculated the electron density using the independent atom model (IAM) for $CuSbSe_2$ and determined the corresponding local energies densities. The results are depicted in Fig. 10 together with those obtained with the relaxed electron density (SCF). As can be seen, for identical bond distances, the absolute value of the slope G_b/ρ_b differs from SCF to IAM. This shows that, G_b/ρ_b is solely related to the electron density.

(a)

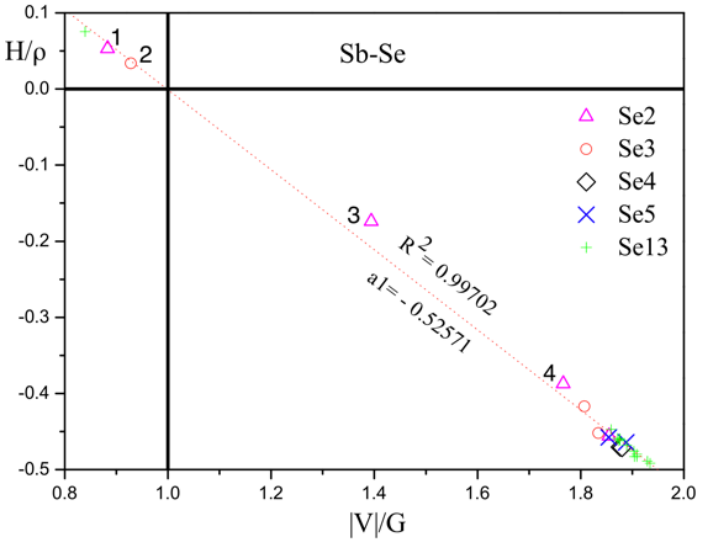

(b)

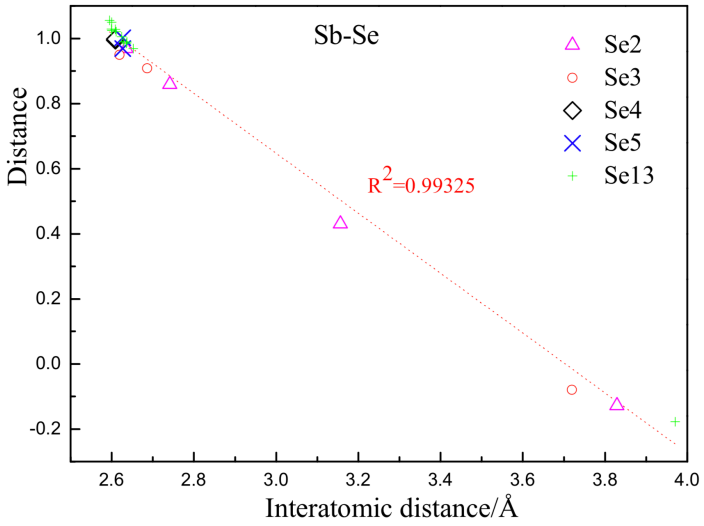

Figure 7. (a) H_b/ρ_b vs $|V_b|/G_b$ of Sb-Se bonding in compounds of the Cu-Sb-Se system; (b) algebraic distance of BCPs to the point (1, 0) in Fig.7(a) vs d(Sb···Se).

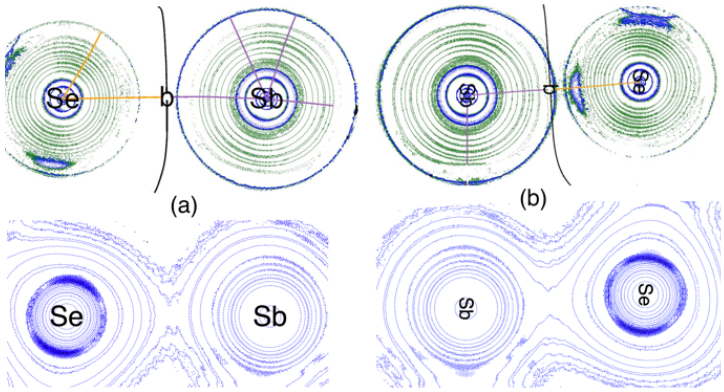

Figure 8. Distribution of $\nabla^2\rho(r)$ (top) and H(r) (bottom) of Sb-Se bonding: (a) and (b) corresponding to points 3 and 4 in Fig.7, respectively.

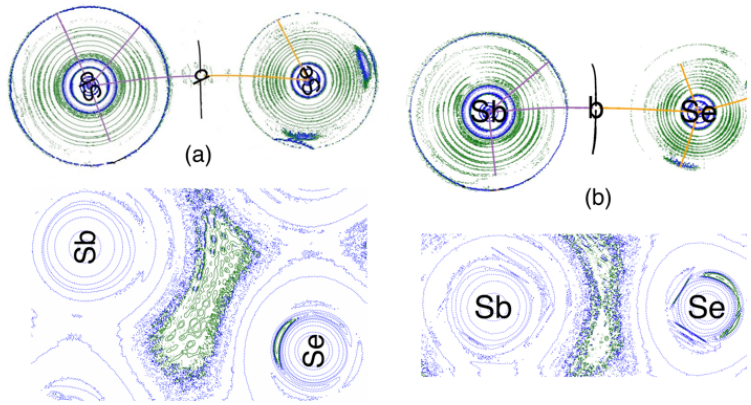

Figure 9. Distribution of $\nabla^2\rho(r)$ (top) and $H(r)/\rho(r)$ (bottom) of Sb-Se bonding: (a) and (b) corresponding to points 1 and 2 in Fig.7, respectively.

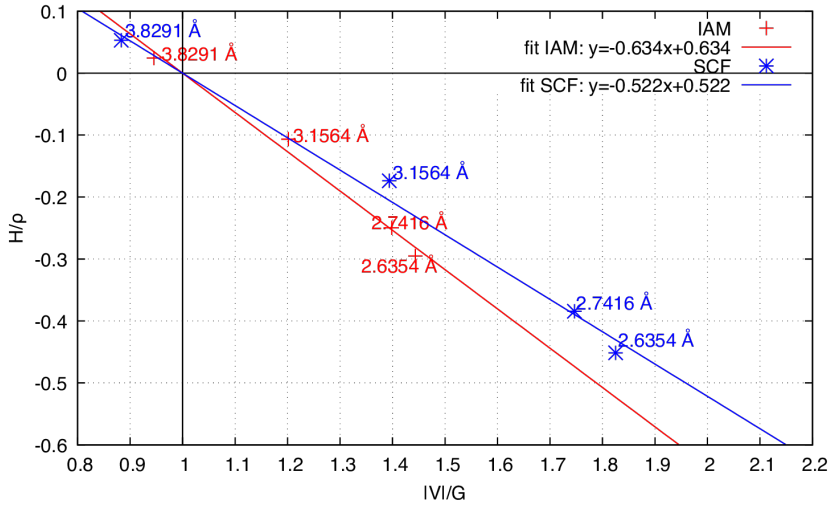

Figure 10. H_b/ρ_b vs $|V_b|/G_b$ for Sb-Se bonding in $CuSbSe_2$. IAM and SCF stand for the independent atom model and self-consistent field, respectively. The numerical values (in Å) correspond to the related inter-atomic distances.

IV. Conclusion

The complete Laplacian shell structure of heavy elements and transition metals has been obtained by calculating the charge density using DFT-PAW approach. By combining the distributions of $\rho(r)$ and $H(r)$ with local properties (energy densities at bond critical point) of interatomic interactions, the Cu-Cu metal bonding, Se-Se bonding in bulk Se, Sb-Sb bonding in bulk Sb and O-O charge-shift bonding in H_2O_2 have been characterized in the real space. This analysis has also been done for chemical bonding in molecules, binary oxides and ternary semiconducting compounds. Specific interactions in a system having similar bonding environment solely determined by interatomic distance presents a linear characteristic of H_b/ρ_b vs $|V_b|/G_b$, the slope G_b/ρ_b being related to the polarizability of the charge distribution and hence to the rigidity of the interaction between the atoms. Hence the energy density analysis at the bond critical point can be used as a rapid method to determine characteristics of a chemical bonding, namely the bonding state, the polarizability and the deformation of the charge distribution.

AUTHOR INFORMATION

Corresponding Author

*(P.B.) E-mail: pascal.boulet@univ-amu.fr.

DECLARATION OF COMPETING INTEREST

The authors declare no competing financial interest.

ACKNOWLEDGMENTS

The authors are grateful to Pr. A. Otero De La Roza for his advices regarding technical aspects of Critic2 program and its usage.

This work is financially supported by China Scholarship Council (CSC). This work was granted access to the HPC resources of the Centre Informatique National de l'Enseignement Supérieur (CINES), Montpellier, France under allocation A0050806881 made by the Grand Equipement National de Calcul Intensif (GENCI). It was also granted access to the HPC resources of Aix-Marseille Université financed by the project Equip@Meso (ANR-10-EQPX-29-01) of the program "Investissements d'Avenir" supervised by the Agence Nationale de la Recherche.

REFERENCES

[1] T.S. Koritsanszky, P. Coppens, Chemical applications of X-ray charge-density analysis. Chem. Rev. 101 (2001) 1583-1628.

[2] R.F. W. Bader, Atoms in molecules: a quantum theory; Oxford University Press, 1990.

[3] T. Koritsanszky, J. Buschmann, P. Luger, Topological analysis of experimental electron densities. 1. The different C-C bonds in Bullvalene. J. Phys. Chem. 100 (1996) 10547-10553.

[4] P. Macchi, D.M. Proserpio, A. Sironi, Experimental electron density in a transition metal dimer: metal-metal and metal-ligand bonds. J. Am. Chem. Soc. 120 (1998) 13429-13435.

[5] M.A. Spackman, A.S. Brown, Charge densities from X-ray diffraction data. Annu. Rep. Prog. Chem., Sect. C: Phys. Chem. 91 (1994) 175-212.

[6] M. Souhassou, R. H. Blessing, Topological analysis of experimental electron densities. J. Appl. Crystallogr. 32 (1999) 210-217.

[7] W. Scherer, M. Spiegler, B. Pedersen, B. Pedersen, M. Tafipolsky, W. Hieringer, B. Reinhard, A.J. Downs, G. S. McGradyet, Molecular recognition in the solid state: topology of experimental and theoretical charge densities for Tetrasulfur Tetranitride. Chem. Commun. (2000) 635-636, https://doi.org/10.1039/A910209O.

[8] M. Messerschmidt, A. Wagner, M.W. Wong, Atomic properties of N_2O_4 based on its experimental charge density. J. Am. Chem. Soc. 124 (2002) 732-733.

[9] P. Mori-Sánchez, A.M. Pendás, V. Luaña, A classification of covalent, ionic, and metallic solids based on the electron density. J. Am. Chem. Soc. 124 (2002) 14721-14723.

[10] P. Macchi, A. Sironi, Chemical bonding in transition metal carbonyl clusters: complementary analysis of theoretical and experimental electron densities. Coord. Chem. Rev. 238 (2003) 383-412.
[11] J. Oddershede, S. Larsen, Charge density study of naphthalene based on X-ray diffraction data at four different temperatures and theoretical calculations. J. Phys. Chem. A 108 (2004) 1057-1063.
[12] P. Coppens, A. Volkov, The interplay between experiment and theory in charge-density analysis. Acta Crystallogr. Sect. A: Found. Crystallogr. 60 (2004) 357-364.
[13] M. Messerschmidt, S. Scheins, L. Grubert, Electron density and bonding at inverted carbon atoms: an experimental study of a [1.1.1] propellane derivative. Angew. Chem. Int. Ed. 44 (2005) 3925-3928.
[14] M. Jablonski, M. Palusiak, Basis set and method dependence in quantum theory of atoms in molecules calculations for covalent bonds. J. Phys. Chem. A 114 (2010)12498-12505.
[15] C. F. Matta, How dependent are molecular and atomic properties on the electronic structure method? Comparison of Hartree-Fock, DFT, and MP2 on a biologically relevant set of molecules. J. Comput. Chem. 31 (2010) 1297-1311.
[16] A. A. Rykounov, V. G. Tsirelson, Quantitative estimates of transferability of the QTAIM descriptors. Case study of the substituted hydropyrimidines. J. Mol. Struct. (Theochem) 906 (2009) 11-24.
[17] V.G. Tsirelson, P.F. Zhou, T.H.Tang, Topological definition of crystal structure: determination of the bonded interactions in solid molecular chlorine. Acta Crystallogr. Sect. A: Found. Crystallogr. 51 (1995) 143-153.
[18] G.V. Gibbs, A.F. Wallace, D.F. Cox, Role of directed van der Waals bonded interactions in the determination of the structures of molecular arsenate solids. J. Phys. Chem. A 113 (2009) 736-749.
[19] V. Luana, A. Costales, A.M. Pendás, Ions in crystals: the topology of the electron density in ionic materials. II. The cubic alkali halide perovskites. Phys. Rev. B 55 (1997) 4285-4297.
[20] Y.A. Abramov, Secondary interactions and bond critical points in ionic crystals. J. Phys. Chem. A 101 (1997) 5725-5728.
[21] J. Cioslowski, S.T. Mixon, Universality among topological properties of electron density associated with the hydrogen-hydrogen nonbonding interactions. Can. J. Chem. 70 (1992) 443-449.
[22] C.F. Matta, J. Hernández-Trujillo, T.H. Tang, Hydrogen-hydrogen bonding: a stabilizing interaction in molecules and crystals. Chem. - Eur. J. 9 (2003) 1940-1951.
[23] U. Koch, P.L.A. Popelier, Characterization of CHO hydrogen bonds on the basis of the charge density. J. Phys. Chem. 99 (1995) 9747-9754.
[24] E. Espinosa, E. Molins, C. Lecomte, Hydrogen bond strengths revealed by topological analyses of experimentally observed electron densities. Chem. Phys. Lett. 285 (1998) 170-173.
[25] Y. Aray, J. Rodriguez, D.Vega, Topology of the electron density and cohesive energy of the face-centered cubic transition metals. J. Phys. Chem. B 104 (2000) 4608-4612.

[26] G.V. Gibbs, R.T. Downs, C.T.Prewitt, Electron density distributions calculated for the nickel sulfides millerite, vaesite, and heazlewoodite and nickel metal: a case for the importance of Ni-Ni bond paths for electron transport. J. Phys. Chem. B 109 (2005) 21788-21795.

[27] G. Gervasio, R. Bianchi, D.Marabello, About the topological classification of the metal-metal bond. Chem. Phys. Lett. 387 (2004) 481-484.

[28] L. Rincón, R. Almeida, On the topology of the electron charge density at the bond critical point of the electron-pair bond. J. Phys. Chem. A 102 (1998) 9244-9254.

[29] L. Zhang, F. Ying, W. Wu, Topology of electron charge density for chemical bonds from valence bond theory: a probe of bonding types. Chem. - Eur. J. 15 (2009) 2979-2989.

[30] J. Hernández-Trujillo, R.F.W. Bader, Properties of atoms in molecules: atoms forming molecules. J. Phys. Chem. A 104 (2000) 1779-1794.

[31] D. Cremer, E. Kraka, Chemical bonds without bonding electron density-does the difference electron-density analysis suffice for a description of the chemical bond? Angew. Chem. Int. Ed. 23 (1984) 627-628.

[32] P.J. MacDougall, R.F.W. Bader, Atomic properties and the reactivity of carbenes. Can. J. Chem. 64 (1986) 1496-1508.

[33] W. Wu, J. Gu, J. Song, The inverted bond in [1.1.1] propellane is a charge-shift bond. Angew. Chem. Int. Ed. 48 (2009) 1407-1410.

[34] P.T.T. Wong, E. Whalley, The intensities of the infrared-active intermolecular translational bands in solid chlorine. Evidence for intermolecular bonding. Can. J. Phys. 50 (1972) 1856-1861.

[35] S. Jenkins, Direct space representation of metallicity and structural stability in SiO solids. J. Phys.: Condens. Matter 14 (2002) 10251-10263.

[36] S. Jenkins, P.W. Ayers, S.R. Kirk, Bond metallicity of materials from real space charge density distributions. Chem. Phys. Lett. 471 (2009) 174-177.

[37] R.F.W. Bader, W.H. Henneker, P.E. Cade, Molecular charge distributions and chemical binding. J. Chem. Phys. 46 (1967) 3341-3363.

[38] C. Gatti, Chemical bonding in crystals: new directions. Z. Kristallogr. - Cryst. Mater. 220 (2005) 399-457.

[39] A.R. Oganov, G. Saleh, A.G. Kvashnin, Computational Materials Discovery; The Royal Society of Chemistry, 2018.

[40] P. Giannozzi, S. Baroni, N.J.Bonini, QUANTUM ESPRESSO: a modular and open-source software project for quantum simulations of materials. Phys.: Condens. Matter 21 (2009) 395502.

[41] P. Giannozzi, O. Andreussi, T. Brumme, Advanced capabilities for materials modelling with Quantum ESPRESSO. J. Phys.: Condens. Matter 29 (2017) 465901.
[42] J.P. Perdew, K. Burke, M. Ernzerhof, Generalized gradient approximation made simple. Phys. Rev. Lett. 7 (1996) 3865-3868.
[43] P.E. Blöchl, Projector augmented-wave method. Phys. Rev. B 5 (1994) 17953-17979.
[44] G. Eickerling, R. Mastalerz, V. Herz, W. Scherer,H.-J. Himmel, M. Reiher, Relativistic Effects on the Topology of the Electron Density, J. Chem. Theor. Comput. 3 (2007) 2182-2197.
[45] F. Neese, The ORCA program system, Wiley Interdisciplinary Reviews: Computational Molecular Science 2 (2012) 73-78.
[46] F. Neese, Software update: the ORCA program system, version 4.0, Wiley Interdisciplinary Reviews: Computational Molecular Science 8 (2017) e1327.
[47] W. J. Hehre, R. F. Stewart, J. A. Pople, Self‐Consistent Molecular‐Orbital Methods. I. Use of Gaussian Expansions of Slater‐Type Atomic Orbitals, J. Chem. Phys. 51 (1969) 2657.
[48] F. Weigend, R. Ahlrichs, Balanced basis sets of split valence, triple zeta valence and quadruple zeta valence quality for H to Rn: Design and assessment of accuracy, Phys. Chem. Chem. Phys. 7 (2005) 3297.
[49] F. Weigend, Accurate Coulomb-fitting basis sets for H to Rn, Phys. Chem. Chem. Phys. 8 (2006) 1057.
[50] D. Rappoport and F. Furche, Property-optimized Gaussian basis sets for molecular response calculations, J. Chem. Phys. 133 (2010) 134105.
[51] A. Otero-de-la-Roza, E.R. Johnson, V.Luaña, Critic2: A program for real-space analysis of quantum chemical interactions in solids. Comput. Phys. Commun. 18 (2014) 1007-1018.
[52] D.A. Kirzhnits, Quantum corrections to the Thomas–Fermi equation. Sov. Phys. - JETP 5 (1957).
[53] D.A. Kirzhnits, Field theoretical methods in many-body systems. Am. J. Phys. 3 (1967) 1166-1167.
[54] Y.A. Abramov, On the possibility of kinetic energy density evaluation from the experimental electron-density distribution. Acta Crystallogr. Sect. A: Found. Crystallogr. 53 (1997) 264-272.
[55] E. Espinosa, C. Lecomte, E. Molins, Experimental electron density overlapping in hydrogen bonds: topology vs. energetics. Chem. Phys. Lett. 300 (1999) 745-748.
[56] D. Cremer, E. Kraka, A description of the chemical bond in terms of local properties of electron density and energy. Croat. Chem. Acta 57 (1984) 1259-1281.
[57] E. Espinosa, I. Alkorta, J. Elguero, From weak to strong interactions: A comprehensive analysis of the topological and energetic properties of the electron density distribution involving X–H··· F–Y systems. J. Chem. Phys. 117 (2002) 5529-5542.

[58] Z. Shi, R.J. Boyd, The shell structure of atoms and the Laplacian of the charge density. J. Chem. Phys. 88 (1988) 4375-4377.

[59] K.C. Götz, Bond analysis of metal-element interactions in molecules and solids applying embedding and density functional techniques. Ph.D. Thesis, Universität Würzburg, Germany, 2009.

[60] G. Frenking, N. Froehlich, The nature of the bonding in transition-metal compounds. Chem. Rev. 100 (2000) 717-774.

[61] A.V. Morozkin, V.N. Nikiforov, N.Imaoka, Ce–Cu–Sb system at 670/870 K. J. Alloys Compd. 422 (2006) L5-L8.

[62] R.P. Sagar, A.C.T. Ku, J.V.H.Smith, The Laplacian of the charge density and its relationship to the shell structure of atoms and ions. J. Chem. Phys. 88 (1988) 4367-4374.

[63] Y. Akahama, M. Kobayashi, H. Kawamura, Structural studies of pressure-induced phase transitions in selenium up to 150 GPa. Phys. Rev. B 47 (1993) 20-26.

[64] M. Sist, C. Gatti, P. Norby, S. Cenedese, H. Kasai, K. Kato, B. Iversen, High-Temperature crystal structure and chemical bonding in thermoelectric germanium selenide, Chem. Eur. J. 23 (2017) 6888-6895.

[65] Y.F. Lomnytska, O.P. Pavliv, Phase equilibria in the V-Ni-Sb system. Inorg. Mater. 43 (2007) 608-613.

[66] W.R. Busing, H.A. Levy, Crystal and Molecular Structure of Hydrogen Peroxide: A Neutron-Diffraction Study. J. Chem. Phys. 42 (1965) 3054-3059.

[67] S. Shaik, P. Maitre, G.Sini, The charge-shift bonding concept. Electron-pair bonds with very large ionic-covalent resonance energies. J. Am. Chem. Soc. 114 (1992) 7861-7866.

[68] S. Shaik, D. Danovich, B. Silvi, Charge‐Shift Bonding-A Class of Electron‐Pair Bonds That Emerges from Valence Bond Theory and Is Supported by the Electron Localization Function Approach. Chem.-Eur. J. 11 (2005) 6358-6371.

[69] S. Shaik, D. Danovich, W. Wu, Charge-shift bonding and its manifestations in chemistry. Nat. Chem. 1 (2009) 443-449.

[70] R.F.W. Bader, H. Essén, The characterization of atomic interactions. J. Chem. Phys. 80 (1984) 1943-1960.

[71] R.M. Imamov, Z.G. Pinsker, Determination of the crystal structure of CuSbSe. Sov. Phys.- Crystallogr. 9 (1965) 721-723.

[72] A. Pfitzner, Cu_3SbSe_3: Synthese und Kristallstruktur. Z. Anorg. Allg. Chem. 621 (1995) 685-688.

[73] A. Pfitzner, Crystal structure of tricopper tetraselenoantimonate(V], Cu_3SbSe_4. Z. Kristallogr. Cryst. Mater. 209 (1994) 685-685.

[74] Y. Zhang, V. Ozolins, D. Morelli, Prediction of new stable compounds and promising thermoelectrics in the Cu-Sb-Se system. Chem. Mater. 26 (2014) 3427-3435.